

Northwest Atlantic



Fisheries Organization

Serial No. 480

NAFO SCR Doc. 81/IX/145

SPECIAL MEETING OF SCIENTIFIC COUNCIL - SEPTEMBER 1981

General Overview of the Nature and Use of Satellite Remote Sensing

Data for Fisheries Application

J.F.R. Gower  
Institute of Ocean Sciences  
P. O. Box 6000  
Sidney, B. C. V8L 4B2

Abstract

The paper presents a review of satellite remote sensing relevant to fisheries science or operations. Examples of visible, infrared and microwave images are shown and discussed, and the results from non-imaging sensors are also presented. References are given to recent, more detailed reviews and to research papers.

Introduction

This paper presents examples of satellite data which are useful in furthering our understanding of the oceans. A full review would need to cover a very wide range of different techniques, (see for example the recent special issues of Oceanus, Fall 1981) and I shall concentrate on examples that have special relevance to fisheries, particularly to regional studies of productivity and to related ocean dynamics and operational requirements for wind and wave data.

A number of sensing techniques have now been tested from space. The infrared mapping of sea surface temperature patterns is well known and widely used. Ice and cloud cover are monitored at infrared and visible wavelengths. Data collection from buoys or shore stations via satellites also has many applications. Shorter tests have been conducted with satellite-borne radars for wind and wave measurements and for producing high resolution images of ice and water roughness patterns. These techniques, and that of microwave radiometry, demonstrate how a satellite may collect remote sensing data through clouds, day or night so as to contribute to a regular monitoring or data collection system.

A recent, and still operating, satellite sensor is collecting images showing the changes in water colour associated with the chlorophyll pigment concentration in phytoplankton in the sea. Because of the relevance of this data to primary productivity, and hence to fisheries, I propose to begin with examples of this, and then to continue to measurements of important, but less direct relevance.

#### Satellite measurements of water colour

Landsat images, such as figure 1, have been available through NASA since 1972. The images give 100 meter spatial resolution in 4 spectral bands, two corresponding roughly to green and red light and two in the near infrared at 0.7 to 0.8  $\mu$  and 0.8 to 1.1  $\mu$ . Each image covers an area about 185 km square. The sensitivity and digitization levels are set for land targets having relatively high reflectivity, but figure 1 shows that in coastal areas water colour patterns are sometimes visible, especially where silt-laden river water floats out onto denser sea water to form a spreading plume. In this example the Fraser river water forms a thin (2 - 4 m thick) surface layer on the sheltered waters of the Gulf of Georgia. Images such as this have been used to map the extent of the river plume in different wind and tide conditions and hence to study the influence of the river water on circulation patterns in fisheries and pollution programs.

The area of the plume is large enough to make aerial mapping difficult, but forms a very conveniently sized target for Landsat. The sensitivity of Landsat however does not allow mapping of the more subtle colour changes further away from the river mouth, and the long coverage cycle of the satellite (an orbital path is repeated every 18 days) makes cloud free observations very infrequent. The size of an individual scene is also very small compared to an ocean basin. These disadvantages have greatly restricted use of Landsat data for oceanographic purposes.

On some occasions, however, even sporadic satellite coverage will pick up unusually bright water colour patterns offshore, caused by strong plankton blooms in highly productive conditions. An example of such a pattern is shown in figure 2. This is the green band of a Landsat image taken in the Atlantic, south of Iceland on June 19, 1976. The scene, 185 km across as before, shows part of what is evidently a much more extended plankton bloom in which water with higher surface concentrations of light-scattering phytoplankton returns

more light to the satellite's optical sensor. The pattern is caused by advection of the water in mesoscale turbulent motion, and the average spatial structure of this turbulence can therefore be deduced from such an image (Gower et al, 1980). The characteristic time scales of such a bloom is a few days, and no other image of this event was recorded by the satellite.

Clearly, one can imagine a satellite sensor better designed to map such transient phenomena. A wider angle of view means that areas are covered more often, even on days when the satellite does not pass directly overhead. Greater sensitivity can allow faint water colour changes to be detected, although the light back-scattered by the atmosphere gives a high background to be subtracted. Choice of wavelength bands allows the characteristic water colour variations to be selectively extracted from the data.

A sensor designed to map water colour, the Coastal Zone Color Scanner on Nimbus 7, has been in orbit since 1978. It has demonstrated that colour patterns can be detected over large areas of the ocean, and that the mean surface chlorophyll concentration responsible for the colour changes can be calculated (Hovis et al, 1980, Gordon et al, 1980).

The chlorophyll is present in the phytoplankton which forms the first stage of the biological productivity of the sea. Mapping of the patterns of primary productivity, and studying their long and short term variations is a basic task of ocean ecology. Movement of any colour patterns visible to a satellite can also be used in following ocean currents, and in tracing the mixing and upwelling that bring the nutrients needed for this productivity. To some extent the satellite's usual disadvantage in being restricted to viewing only the ocean surface, is here less important since photosynthesis and hence phytoplankton growth, is similarly restricted to the sunlit near-surface layers. Subsurface maxima of phytoplankton concentration that tend to be formed in highly stratified water, however, will only be imperfectly sensed from above.

Figure 3 shows an example of a Coastal Zone Colour Scanner image. The data is collected in 4 high-sensitivity bands of visible light, each 20 nm wide, in the blue, blue/green, green and red regions of the spectrum (443, 520, 550 and 670 nm). The blue band is at a wavelength where light is strongly absorbed by chlorophyll pigments present in phytoplankton, whereas in the green band, backscattering by the other cellular material in the plankton is the dominating effect. The presence of pigment will therefore be indicated by a decrease in blue radiance, with a corresponding increase in the green.

This change of sea colour, from blue to lighter greens with increasing phytoplankton content, has been familiar to sailors and fishermen for centuries, and has been used for navigation and for locating productive areas. The Coastal Zone Color Scanner has shown that these colour changes can be measured from space and hence monitored regularly over large areas.

To do this accurately, the effect of the atmosphere must be allowed for. The contribution of Rayleigh scattering from atmospheric gases can be calculated, and much of the effect of haze and thin cloud can be deduced from measurements in the red band. At the longer wavelength of this band, increasing absorption by the sea water itself reduces radiance backscattered from below the surface and most of the observed radiance is returned by backscattering in the atmosphere. Especially over relatively clear water, therefore, the radiance in this channel is a measure of the atmospheric contribution alone and can be used to deduce corrections to the other three channels. For more turbid waters some water radiance is still present, and a longer wavelength, infra-red, channel would be needed to give a nearly black background for measurement of the atmospheric signal.

Figures 3(a) and 3(b) show blue and green band images respectively of a cloud free area off the west coast of Vancouver Island on July 14, 1979. These have both been corrected for Rayleigh scattered light and for the effects of thin haze. Note the eddy near the centre of the figure which shows the relative darkness in the blue and brightness in the green, characteristic of increased phytoplankton concentration. Several other areas including a hammerhead feature further south behave similarly.

In figure 4 a ratio of these two images is formed to emphasize such areas. Increased brightness in the green to blue ratio image may then be interpreted as indicating increased chlorophyll. Areas bright in both bands are interpreted as containing more scatterers, but relatively less pigment. Areas dark in both bands are again interpreted according to the value of the ratio, though dissolved organic matter in the fresh water run-off may also be increasing the ratio in the area close to the coast.

A large amount of ocean optics data has now been collected with a view to deriving a quantitative relation between this green to blue ratio and the near surface chlorophyll concentration. The general conclusion has been that in water whose optical properties are dominated by the presence of phytoplankton, the average spectrum of light from the water is related to the chlorophyll

pigment concentration and the diffuse attenuation coefficient as shown in figure 5 (Austin and Petzold, 1981). At low pigment concentrations ( $< 0.1 \text{ mg m}^{-3}$ ) a considerable amount of blue light is scattered back upwards. Up to about  $0.7 \text{ mg m}^{-3}$  the blue light diminishes and at higher levels the reflection for green light increases. The curves in this figure are normalized at 520 nm (blue/green) to remove some of the variations due to broad-band backscatter. These curves represent the water spectral variation that is mapped in the ratio image in figure 4. Water affected by coastal sediment or dissolved organic matter will not behave in the same way, making quantitative determination of chlorophyll more difficult.

The data in figure 5 would suggest that water in the eddy and hammerhead feature contains about  $2 \text{ mg/m}^3$  of chlorophyll pigment with higher values to  $5 \text{ mg m}^{-3}$  near shore and lower values  $< 0.5 \text{ mg/m}^3$  further offshore.

Apart from giving quantitative results of this kind, features visible in figures 3 and 4 suggest a variety of water movements. These include a flow of more productive water south out of Hecate Strait (North of Vancouver Island) with a band of less productive water moving north-west close to the coast. Eddies at the edge of this northwestward flow are visible in the more productive water near the coast of Vancouver Island. Water movement out of Juan de Fuca Strait (South of Vancouver Island) is also suggested by the counter-clockwise eddy of productive water near its mouth, and by the hammerhead feature further offshore.

The thermal infra-red image collected by the AVHRR scanner on NOAA 5 2.5 hours later is shown in figure 6. This shows temperature contrasts due to tidal mixing in inshore waters but very few of the features further offshore that are visible in the colour data.

The water colour images can thus give quantitative data as well as maps of contrasts and boundaries in a manner analogous to thermal infrared images. The above discussion also indicates that the colour data can show structure not previously visible from space.

A large quantity of Nimbus 7 water colour data has now been collected, covering many parts of the world. Figure 7 shows an example of chlorophyll pigment and diffuse attenuation coefficient images for the waters off eastern Canada and north-eastern U.S.A. on June 14, 1979. Atmospheric corrections, followed by fitting to the water radiance spectra illustrated in figure 5 lead to numerical values given against the step wedge beneath the two images.

Georges Bank shows as the more productive area south-east of Cape Cod, and higher pigment values are associated with the Scotian Shelf and other coastal areas. Low pigment values occur in the Gulf Stream at the bottom edge of the image, where the northern tip of a warm core eddy can just be seen.

Several new sensors are being planned for this work, among them the DFO (Canada) Fluorescence Line Imager. This device would make use of solid state imaging techniques to allow measurement of the natural fluorescence signal from chlorophyll a (Gower and Borstad 1981) as well as to improve sensitivity for measurements, such as those illustrated above, based on absorption. Mapping two properties of the chlorophyll a simultaneously should lead to increased accuracy in the results, and may also allow changing properties of the phytoplankton to be studied as it grows and decays.

NASA's Coastal Zone Color Scanner is still in orbit, but is failing fast. Color Sensors planned for NOSS and for the European ERS-1 have been cancelled. The colour data has valuable applications in a number of fields and NASA is presently searching for opportunities to launch a second sensor, with minor improvements, in the near future.

#### Thermal Infrared Mapping

Infrared images showing sea surface temperature contrasts have been available for about 10 years. The data has been used both for temperature determination and for mapping structure and movements. It is collected routinely by weather satellites for cloud imaging, but is less often available in the enhanced form suitable for mapping sea surface temperature features.

An example of an enhanced infrared image is shown in figure 8. Here the thermal contrast between warm Gulf Stream water and cooler shelf water shows up strongly. Processes that mix the two such as large scale instabilities and eddy formation and their effect on the movement of shelf water can be studied from such images as discussed in the paper by Chamberlain in this volume.

The coverage is however strongly limited by cloud, and images showing features east of 60°W are relatively rare. This is a pity, since the dynamics round the tail of the Grand Banks are particularly important for studying shelf water exchange on the Banks, and the interaction of the Laborador current and Gulf Stream forms strong dynamic patterns near Flemish Cap. In fact there is a general tendency for strong thermal contrast on the sea surface to cause cloud

formation, so that many interesting areas round the world will be screened from satellites.

The limitation is equally strong for visible as for thermal infrared radiation. Cloud penetration requires observation at microwave wavelengths using active (radar) or passive (radiometric) techniques. At these wavelengths no "colour" effects remain since microwave quanta are far too weak to stimulate biochemical reaction. Thermal effects can be detected, but surface reflectance variations are usually the dominating influence on the sensor signal.

#### Synthetic aperture radar imagery

Images of surface microwave reflectance variation can be formed with extremely high spatial resolution using synthetic aperture radar (SAR). Returned signals received at successive locations along the satellite's orbit are combined to give a resolution (for Seasat) of 25 meters. This requires combining signals received over about 2 seconds of time, during which the satellite's motion traces out a "synthetic aperture" antenna about 15 km long. The synthesis involved in forming the image is complicated and time consuming for even a specially configured computer. The process assumes that the targets are stationary during the two seconds, and motions or changes such as those due to surface wave motion can lead to blurring, shifting and lack of contrast in the final image. The radar return is preferentially from short waves satisfying the Bragg condition and having roughly the same wavelength as the radar. These waves will form mean roughness patterns that are anisotropic, being caused by wind or longer waves moving in a particular direction. The visibility of surface patterns to a SAR can therefore change, but in general, roughness variations due to surface or internal wave motion, wave refraction at current boundaries, wind variation, or atmospheric boundary layer stability changes can be imaged with high geometric precision. Several examples exist where the SAR imagery shows effects of currents flowing over varying bottom topography, or the results of the shear patterns in the Gulf Stream (Hayes, 1981) or in warm core eddies. (Lichy et al, 1981).

The more dramatic changes due to sea ice or coastlines will generally show clearly, but since the mean roughness of the sea varies with wind speed, the contrast is not fixed. Figure 9 shows an example of a Seasat SAR image in which smooth shorefast ice and offshore floes give low returns and appear dark, the rougher shore lead appears grey, but even rougher areas, probably rubble fields, in the ice pack further offshore, give greater radar return and show

brighter. A different choice of radar incidence angle can improve the ice/water contrast situation in future systems, and SAR can certainly be usefully applied to mapping sea ice.

Because of the high spatial resolution achieved, Seasat SAR images show surface wave patterns down to wavelengths of 50 to 100 meters whose mean length and direction agrees well with surface observations (Gonzales et al, 1981 Vesecky et al, 1981). In fact, since surface observations are limited by the inherent randomness of the wave field we might expect that the satellite image can give a superior indication of these two parameters, although direction can only be deduced with a two-fold ambiguity since the satellite image only shows wave "crest" lines.

Figure 10 shows an example of such a SAR image in which surface waves travelling from the west (left to right on the image) are diffracted round Sumburgh Head at the southern tip of the Shetland Islands northeast of Scotland. The ocean waves here have a mean wavelength of 200 meters, well within the capability of a radar having 25 m resolution. In this rather special case the diffraction solves the direction ambiguity problem.

Other information on the wave spectrum can be deduced from such images. To some extent the lengths of the crest lines indicate the angular width in the wave spectrum. A spatial frequency analysis (two dimensional Fourier transform) can show several wavelength components, possibly moving in different directions. The complete wave spectrum would only be produced if the radar image brightness were linearly related to sea surface height at each point. Since the relation should involve slope, surface convergence and motion as well as being dependent on the surface wind, a full, simple answer cannot be expected. Comparisons show, however, that the peak wave components are accurately mapped, but with a variable lower limit of wave height which depends on the look direction. Detection of shorter waves depends critically on maintaining the full spatial resolution of the radar through precise processing.

Other roughness patterns caused by ocean dynamics or boundary layer effects are visible in SAR images, especially at low wind speeds. Internal waves, fronts and eddies, rain cells and surface wind patterns have all been mapped. The volume edited by Beal et al (1981) provides a good review with examples.

The combination of satellite power, data band width and processing throughput limits the coverage of SAR imagery. Seasat gave narrow swaths

in a pattern that would take roughly 25 days for full earth coverage. Separated swaths of wave data from such a pattern could be used as input to a directional, spectral wave model, but for operational wave model input a map of surface wind velocity would be more useful. The scatterometer on Seasat was designed to provide such wind data.

#### Scatterometer measurements of wind speed

A scatterometer measures the directional properties of the microwave reflectivity caused by wind induced roughness of the sea surface (Jones et al, 1981).

This roughness is anisotropic in the sense that for oblique viewing the measured cross wind microwave reflectivity is less than that in the upwind or downwind direction. The Seasat scatterometer measured reflectivity of elements of the sea surface in two azimuths at right angles, using four beams each with incidence angles of  $20^{\circ}$  to  $50^{\circ}$ . Use of Doppler information provided a spatial resolution of 50 km over a swath 500 km wide, beginning 200 km from nadir, on each side of the spacecraft. If both measured reflectivities are equal, then the wind direction must be between the two azimuths of measurement or at right angles to this, leading to a fourfold ( $90^{\circ}$ ) ambiguity. If the two reflectivities differ by the maximum value expected from measurements of the anisotropy, then the wind direction is identified with only twofold ( $180^{\circ}$ ) ambiguity since the direction with higher reflectivity must be upwind or downwind. In the more general case, a smaller measured difference leads to a fourfold ambiguity of direction, two  $180^{\circ}$  ambiguities separated by an acute angle.

The instrument met its goal of providing wind speeds within  $\pm 2$  m/sec or 10% of surface measurements, and directions within  $\pm 20^{\circ}$  when some external means of ambiguity removal was used. The scatterometer has the advantage of providing a spatially averaged measurement, so avoiding problems with random fluctuations in the wind field. Also, the surface reflectivity may be providing a better measurement of surface wind stress as needed for wave forecasting, than of wind speed, though this has not been tested directly.

Figure 11 shows an example of the scatterometer data plotted to show the patterns of surface wind. Numbers give the measured speed, and short lines indicate possible directions with the two- or four-fold ambiguity. Studies of data (NASA, 1980) show that patterns of cyclones, anticyclones and cols can be identified and plotted in spite of the ambiguities without making use of any other information. The resulting locations are superior to those deduced from

satellite cloud images in which high level cloud can obscure surface features. Scatterometer coverage is much denser than that from conventional, ship observations, and frequent examples have been found where scatterometer data would have improved standard analyses.

Scatterometer data from a single satellite could provide sufficient wind data input for a suitably designed directional wave model. An improved instrument of the Seasat type was planned for NOSS, but now that this has been cancelled we must await future European or Japanese developments.

#### Microwave Radiometry

The ocean emits thermal energy in the microwave region of the spectrum as well as in the infrared. Because such energy is relatively unaffected by clouds, all weather sea surface temperature mapping can be attempted (Hofer, et al, 1981; Njoku and Hofer, 1981). The signal is affected by surface and atmospheric conditions, most importantly roughness and cloud water content, but the instruments on Seasat and Nimbus 7 demonstrated that a multichannel scanning radiometer can separate out the confusing effects into separate maps of water temperature, surface wind speed, atmospheric water vapour and cloud water content (Njoku and Hofer, 1981; Chang et al, 1981). Over ice a similar separation into the fractional cover of multi-year and first year ice also seems possible (Gloersen et al, 1981). The spatial resolution of such maps will be low, depending on the lowest microwave frequency needed. In the calculations for water temperature the Seasat and Nimbus 7 "SMMR" instruments, observing at 6.6 GHz, averaged over 130 km. For NOSS a much larger (4 m) antenna was planned which would have reduced this to about 35 km.

Under moderate conditions the passive microwave data is able to measure temperature to about the same accuracy as infrared sensors while having the great advantage of cloud penetration. The measurements are strongly affected by sun glint and man-made interference, both of which will limit their usefulness in an operational system. Wind measurements, giving speed only, are about as accurate as for the scatterometer.

The information that the radiometer gives on atmospheric properties, particularly water content, is useful in correcting for absorption of scatterometer signals and for delay of the altimeter pulses. Radiometers may therefore be included in an auxiliary role for this purpose.

Figure 12 shows results calculated from SEASAT radiometer data as the

satellite passed over Hurricane Fico in the Pacific ocean on July 20, 1978. The winds calculated from the radiometer are here compared with those derived from scatterometer data. They agreed well except near the centre of the hurricane. Here the radiometer shows high liquid water, whose attenuation would be expected to reduce the scatterometer return signal, and lead to erroneously low results if uncorrected. The surface temperatures indicated here may also be affected by the water vapour content of the atmosphere; the algorithms are still being refined.

Relatively large salinity changes, on the order of 0.2 to 1 parts per thousand, can also be sensed by low frequency radiometers operating below about 2 GHz in frequency. Here however the problems of low spatial resolution become more extreme, though it is possible that a large microwave dish, about 100 m in diameter, could map surface salinities on a 2km scale some time in the future. Radiofrequency interference would still be a major problem. At present there are no plans to launch such an instrument into space although much smaller airborne measurements have demonstrated the principle (Kendall and Blanton, 1981).

#### Altimeter measurements of the sea surface

An altimeter measures the total travel time for a microwave pulse, transmitted downwards and reflected back to the satellite from the ocean surface directly beneath. Since this pulse width can be equivalent to about 0.5 metres of range difference, its shape will be strongly distorted by reflection from points at different heights on the sea surface (Townsend et al, 1981). This pulse shape is recorded, and used to give a direct measurement of the distribution of surface height, from which the significant waveheight,  $H_{1/3}$ , can be computed. The distribution is measured over a circular area centred on the nadir, of radius 1.2 to 6 km depending on the waveheight. The spatial averaging reduces the effect of random fluctuations in the wavefield, to roughly the same extent as the 20 minutes of temporal averaging common in analysing waverider records. Further spatial averaging is possible as the satellite proceeds along its track.

The Seasat altimeter gave waveheight measurements to 10% or 0.5 m, and estimates of its accuracy are largely limited by that of conventional buoy and ship data.

This waveheight data is only available for points directly beneath the satellite so that in one day, coverage is along the lines of a very coarse

grid with spacing of about 3000 km. This is still a large amount of wave data, of higher quality than that provided by standard ship reports, and could contribute to wave modelling and forecasting.

The altimeter's range measurements, when corrected for the satellite's orbital positions and the precise shape of the local geoid, show sea surface mean height variations related to major ocean current systems such as the Gulf Stream. The geostrophic balance of an ocean current on a rotating earth implies a slope of the sea surface proportional to the water speed. At the north-west wall of the Gulf Stream there is a one meter height change over several kilometers. Comparisons of the surface height and the wave height measurements (Townsend et al 1981) show cases in which the waveheights appear strongly related to the current, presumably due to wave/current interaction. (Figure 13). Such effects are a well known, but poorly defined hazard for ocean operations.

Other features of the sea surface height profile, measured by an altimeter beneath the satellite, can be related to the vertically integrated motion in eddies (Cheney and Marsh, 1981). Figure 14 shows examples of altimeter measurements over a repeated track as a cold eddy drifts slowly past. Passage of an eddy would be seen even if the eddy were capped by warmer Sargasso sea water.

The precision of the satellite altimeters has progressed from about 25 cm for GEOS-3 to about 5 cm for Seasat. The NOSS instrument would have been similar to Seasat, but a major new project planned to measure the circulation of the world's oceans (Topex) would aim for 2 cm. The Gulf Stream was detected by the GEOS-3 satellite and accurately measured by Seasat. The return flows in the Atlantic however, give very much smaller slopes, and make the full precision of Topex necessary. Such precision can only be achieved by careful attention to satellite tracking in a specially selected, stable orbit, to gravity determinations using an associated Gravsat experiment, and to correction for atmospheric loading and propagation delay. Scatterometer measurements at the same time are also required so that the current measurements can be interpreted in terms of wind forcing.

The total project is a major one, but would dramatically improve our knowledge of ocean dynamics. The proposed period is five years, so that over this time, variability could be related to observed year class changes in different fisheries, for example. Such a project also gives new information on ocean heat budgets for studying and predicting climatic changes on longer

time scales.

#### General Conclusions

The above survey discusses a variety of remote sensing data from the biologically related colour measurements to the large scale general circulation studies. All could have important applications to fisheries science or operations, but all are in a more or less developmental phase, and in some cases the necessary satellite sensor is not now in orbit. The potential of satellites has, however, been demonstrated.

Full realization of this potential takes time. After a sensing technique has been tested and found useful there will be several years before it is in widespread use, even for the direct and graphic example of thermal infrared imagery. This surface temperature data has been available from weather satellites for over ten years, but few users have sufficient (or sufficiently cheap) receiving and computing capability to make the fullest use of it. This only comes with the ability to store large amounts of data, correct it and rectify it to a common geometrical grid and then to map trends and movements. The data-collecting capabilities of satellite remote sensing makes necessary an improvement and cheapening of processing equipment equivalent to one, or perhaps two, generations of improving technology.

This technology is expanding rapidly and use of satellite data can in future dramatically expand. The major uncertainty is in funding for launch of new satellites. International cooperation, here as in other areas, may be our salvation.

#### REFERENCES

- Austin, R. W., and T. J. Petzold, 1981. "The determination of the diffuse attenuation coefficient of sea water using the Coastal Zone Color Scanner," in "Oceanography from Space." J.F.R. Gower, Ed. Plenum Press, New York. pp. 239-256
- Beal, R. C., P. S. de Leonibus and I. Katz, 1981. "Spaceborne synthetic aperture radar for oceanography." Johns Hopkins University Press, Baltimore.
- Chang, A.T.C., T. T. Wilheit and P. Gloersen. 1981. "Global maps of atmospheric water vapor, cloud water and rainfall derived from Nimbus 7 Scanning Multichannel Microwave Radiometer Data: a Case Study" in "Oceanography from Space." J.F.R. Gower, Ed., Plenum Press, New York. pp. 683-689
- Cheney, R. E. and J. G. Marsh, 1981 "Seasat Altimeter Observations of Dynamic Topography in the Gulf Stream Region." Journal of Geophysical Research, 86, 473-483

- Gloersen, P., W. J. Campbell and D. Cavalier. 1981. "Global maps of sea ice concentration, age and surface temperature derived from Nimbus 7 scanning multichannel microwave radiometer data: a case study," in "Oceanography from Space." J.F.R. Gower, Ed., Plenum Press, New York, pp. 777-783
- Gonzales, F. I., R. A. Schuchman, D. B. Ross, C. L. Rufenach and J.F.R. Gower, "Synthetic aperture radar observations during GOASEX," in "Oceanography from Space." J.F.R. Gower, Ed., Plenum Press, New York. pp. 459- 467
- Gordon, H. R., D. K. Clark, J. L. Mueller, and W. A. Hovis, 1980. "Phytoplankton pigments from the Nimbus 7 Coastal Zone Color Scanner's comparisons with surface measurements." *Science*, 210, 63-66
- Gower, J.F.R., K. L. Denman and R. T. Holyer, 1980. "Phytoplankton patchiness indicates the fluctuation spectrum of mesoscale oceanic structure." *Nature*, 288, 157-159
- Gower, J.F.R. and G. Borstad, 1981. "Use of the in vivo fluorescence line at 685 m for remote sensing surveys of surface chlorophyll a" in "Oceanography from Space." J.F.R. Gower, Ed., Plenum Press, New York. pp 329-338
- Hayes, R. M., 1981. "Detection of the Gulf Stream" in "Spaceborne synthetic aperture radar for oceanography." R. C. Beal, P. de Leonibus, I. Katz, Eds., Johns Hopkins University Press, Baltimore, pp. 146-160
- Hofer, R., E. G. Njoku and T. W. Waters, 1981. "Microwave radiometric measurements of sea surface temperature from the Seasat satellite: first results, *Science*, 212, 1385-1387
- Hovis, W. A., D. K. Clark, F. Anderson, R. W. Austin, W. H. Wilson, E. T. Baker, D. Ball, H. R. Gordon, J. L. Mueller, S. Z. El-Sayed, B. Sturm, R. C. Wrigley and C. S. Yentsch, 1980, "Nimbus 7 Coastal Zone Color Scanner: system description and initial imagery," *Science* 210, 60-63
- Jones, W. Linwood, F. J. Wentz and L. C. Schroeder, 1981. "Microwave scatterometer measurements of oceanic wind vector," in "Oceanography from Space." J.F.R. Gower, Ed., Plenum Press, New York. pp. 553-562
- Kendall, B. M., and J. O. Blanton, 1981. "Microwave radiometer measurement of tidally induced salinity changes off the Georgia coast." *Journal of Geophysical Research*, 86, 6435-6441
- Lichy, D. E., M. G. Mattie and L. J. Mancini, 1981. "Tracking of a warm water ring" in "Spaceborne synthetic aperture radar for oceanography." R. C. Beal, P. De Leonibus, I. Katz, Eds., Johns Hopkins University Press, Baltimore. pp. 171-182
- NASA, 1980, "Seasat-JASIN Workshop Report," Vol. 1. JPL publication 80-62.
- Njoku, E. G., and R. Hofer. 1981. "Seasat SMMR observations of ocean surface temperature and wind speed in the north Pacific," in "Oceanography from Space." J.F.R. Gower, Ed. Plenum Press, New York. pp. 673-681
- Townsend, W. F., J. T. McGoogan and E. J. Wash. 1981. Satellite radar altimeters--present and future oceanographic capabilities." in "Oceanography from Space." J.F.R. Gower, Ed. Plenum Press, New York. pp. 625-636
- Vesecky, J. F., M. M. Assal, R. H. Stewart. 1981. "Remote sensing of the ocean waveheight spectrum using synthetic aperture radar images," in "Oceanography from Space." J.F.R. Gower, Ed., Plenum Press, New York. pp. 449-457

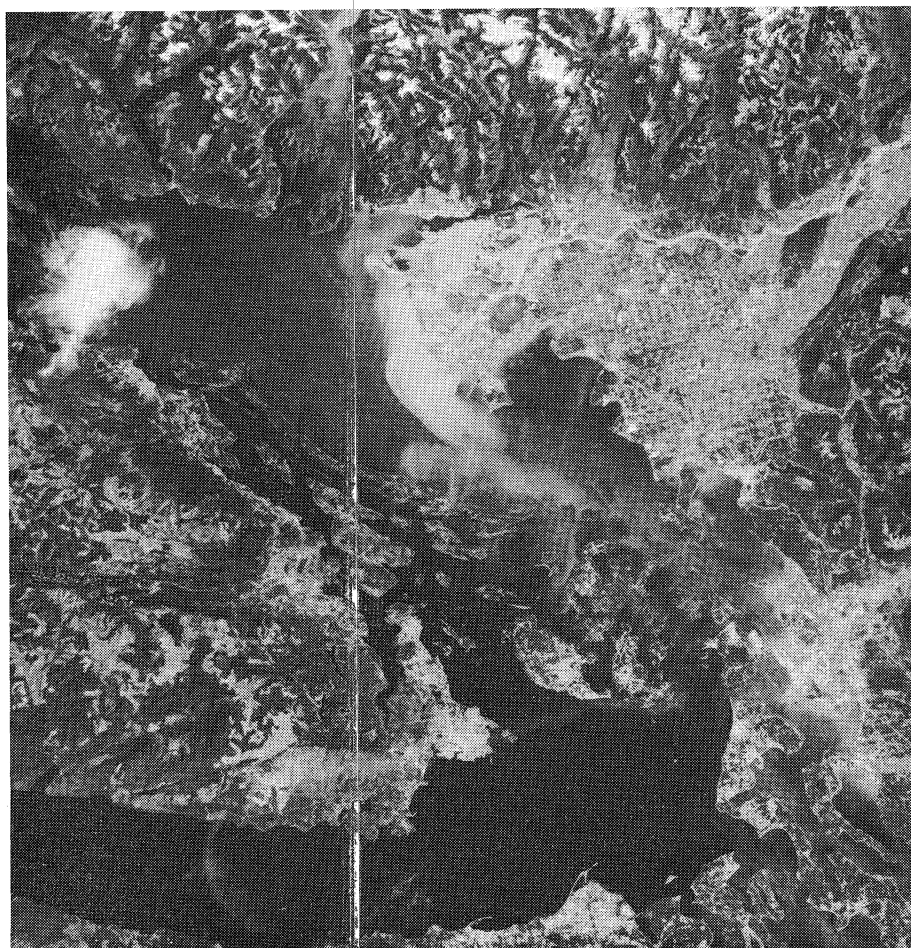


Fig. 1. A Landsat Multi Spectral Scanner image showing the Vancouver/Victoria area of British Columbia, Canada on 30 July 1972 in the red region of the visible spectrum (600 to 700 nm). The plume of silty water from the Fraser River is clearly visible in the centre of the scene. There is one cloud over the Strait of Georgia at the top left of the scene. Some thin haze patterns, for example over Juan de Fuca Strait near the bottom of the scene, are difficult to distinguish from water colour changes in a single band image.

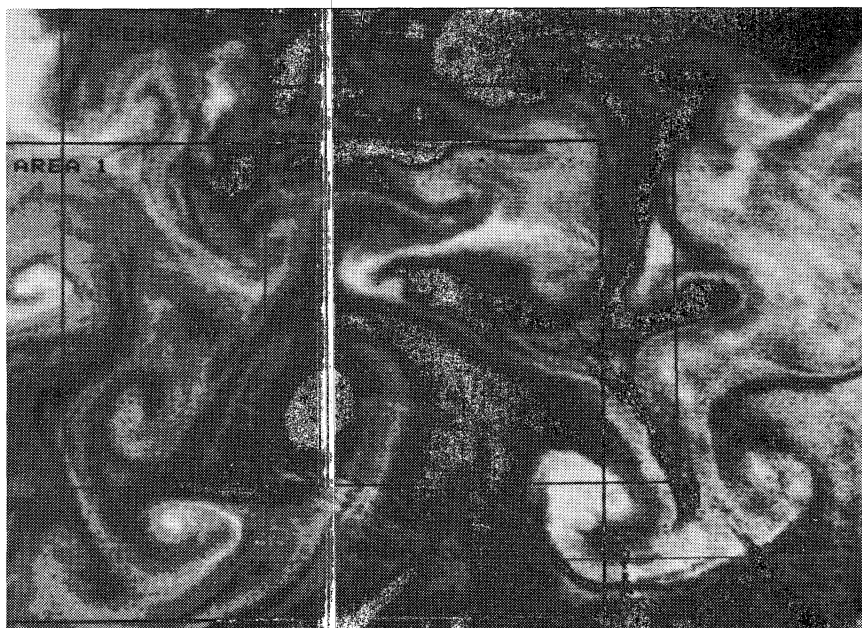


Fig. 2. An enhanced green band (400 to 500 nm) Landsat scene showing increased water reflectance in the Atlantic ocean south of Iceland on 19 June 1976. The patterns are interpreted as due to a plankton bloom in water advected by meso-scale turbulence. Haze patterns have been reduced using image data in the longer wavebands, but some dark and light streaks remain. The 'areas' shown were used in the spectral analysis.



Fig. 3A. Coastal Zone Color Scanner blue band image of a cloud-free area west of Vancouver Island on 14 July 1979, showing water colour patterns where increasing phytoplankton content leads to less brightness because of light absorption by chlorophyll pigments.

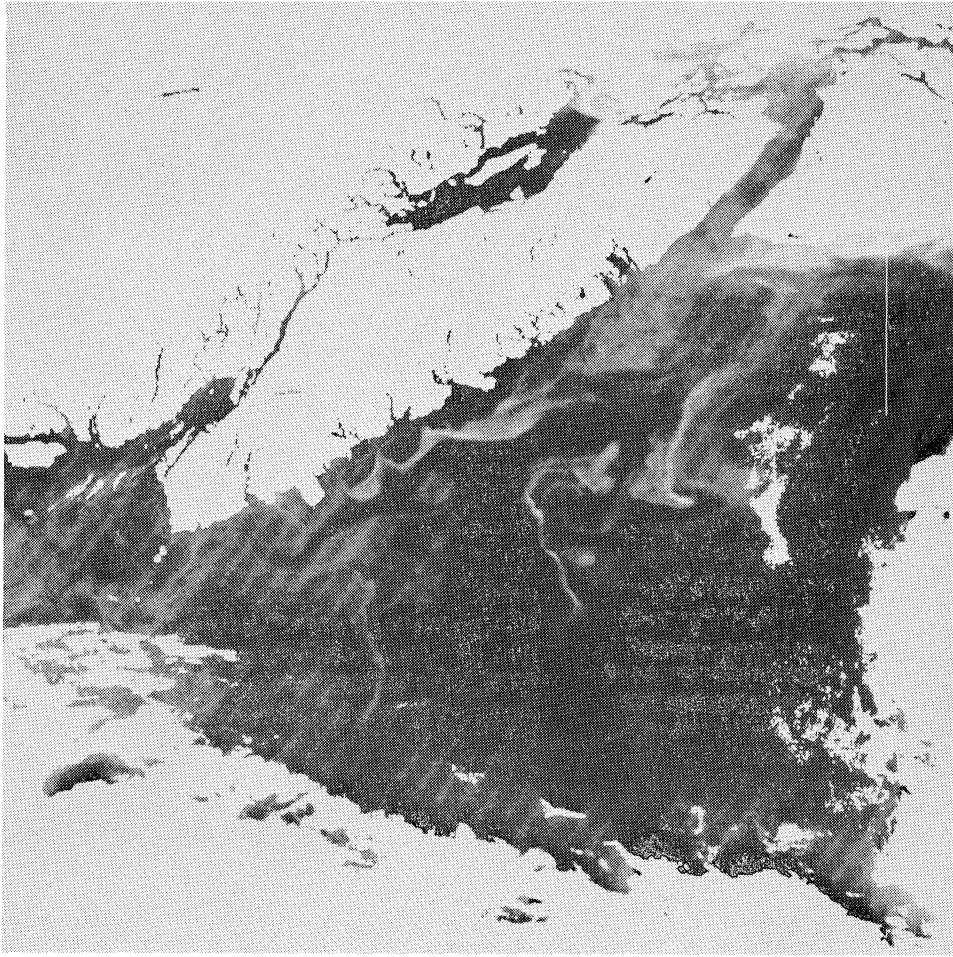


Fig. 3B. The same Coastal Zone Color Scanner image as in Fig. 3A, but in the green band, where increasing phytoplankton content leads to more brightness because of back-scattering from other cellular material in the plankton.



Fig. 4. The green to blue ratio image formed by dividing the pixel values of figure 3B by those in figure 3A. The brightness levels of this image can be related to chlorophyll concentration and show that water in the eddy near the centre of the image and in the hammer-head feature further south contain about  $2\text{mg}\cdot\text{m}^{-3}$  of chlorophyll pigment, with higher values to  $5\text{mg}\cdot\text{m}^{-3}$  near shore and lower values,  $<0.5\text{mg}\cdot\text{m}^{-3}$  further offshore.

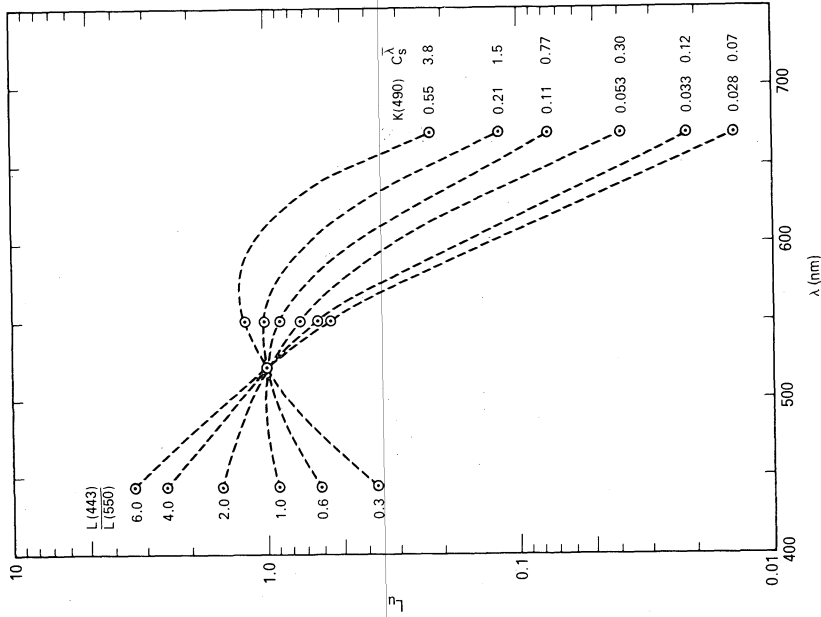


Fig. 5. Upwelling water radiance spectra for sunlight illumination of seawater whose optical properties are dominated by the presence of phytoplankton. These curves are a best fit model to many observations from locations round the world, and are used to interpret the satellite data shown in figures 3 and 4.

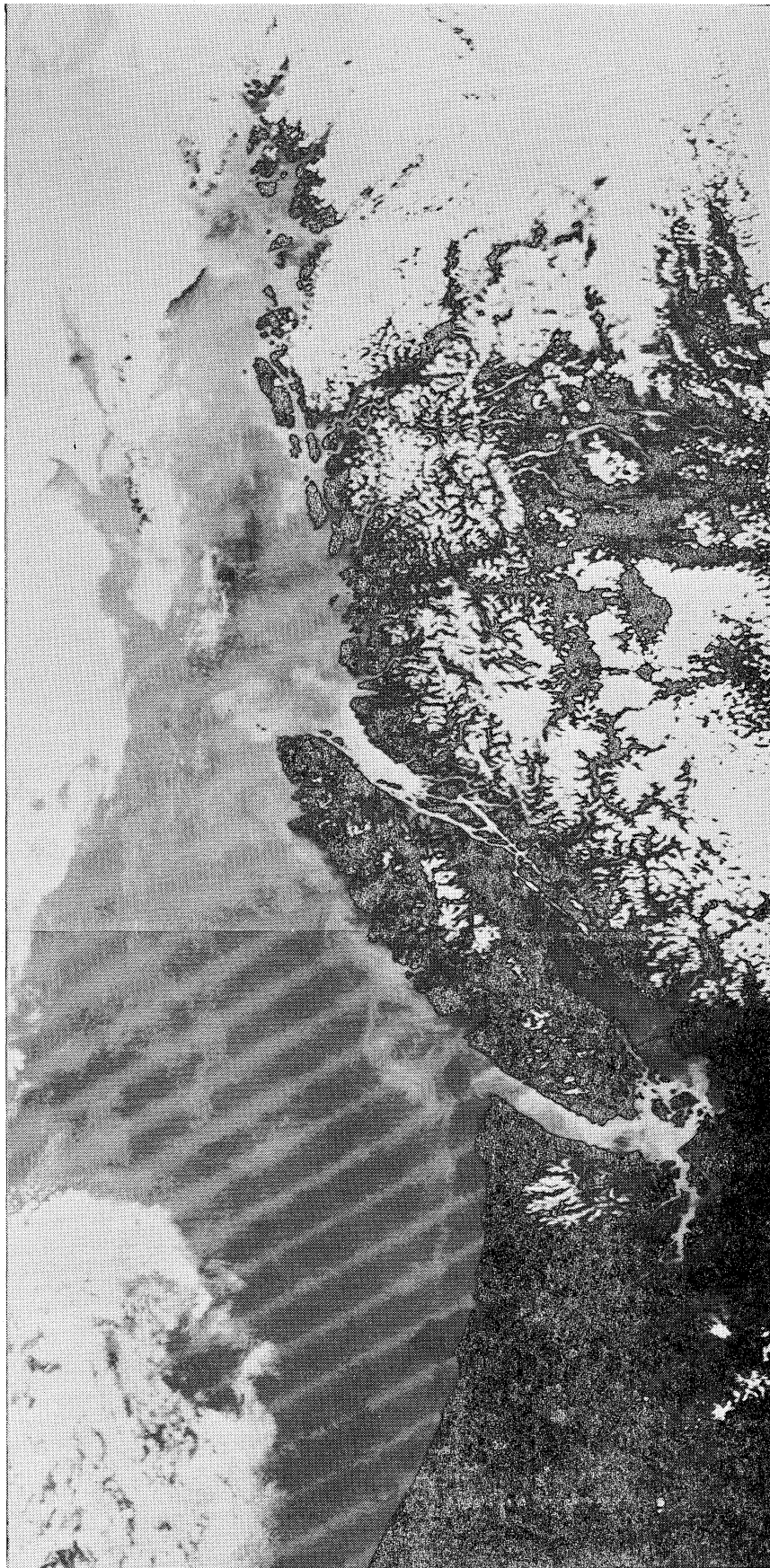


Fig. 6. Thermal infrared imagery from the NOAA 5 AVHRR sensor taken at 2234 GMT on 14 July 1979, or 2.5 hours after figures 3 and 4. Effects of tidal mixing in inshore channels show strongly, but few of the offshore patterns are seen.

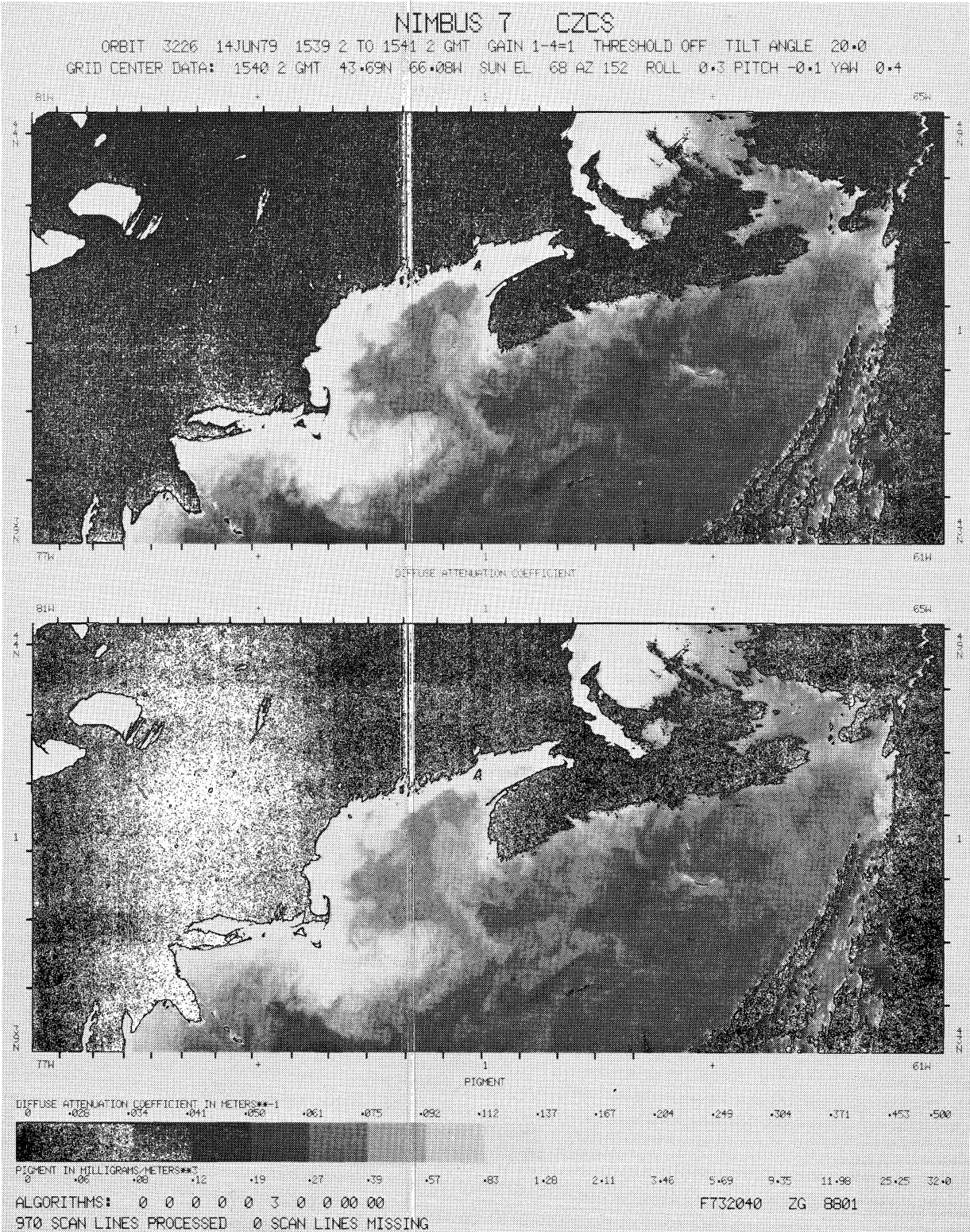


Fig. 7. Chlorophyll pigment and diffuse attenuation coefficient images for the coastal regions of eastern Canada and the U.S. on 14 June 1979. Higher phytoplankton concentration on Georges Bank and in other central areas can be clearly seen. Values for both quantities are given against the step wedge at the bottom.

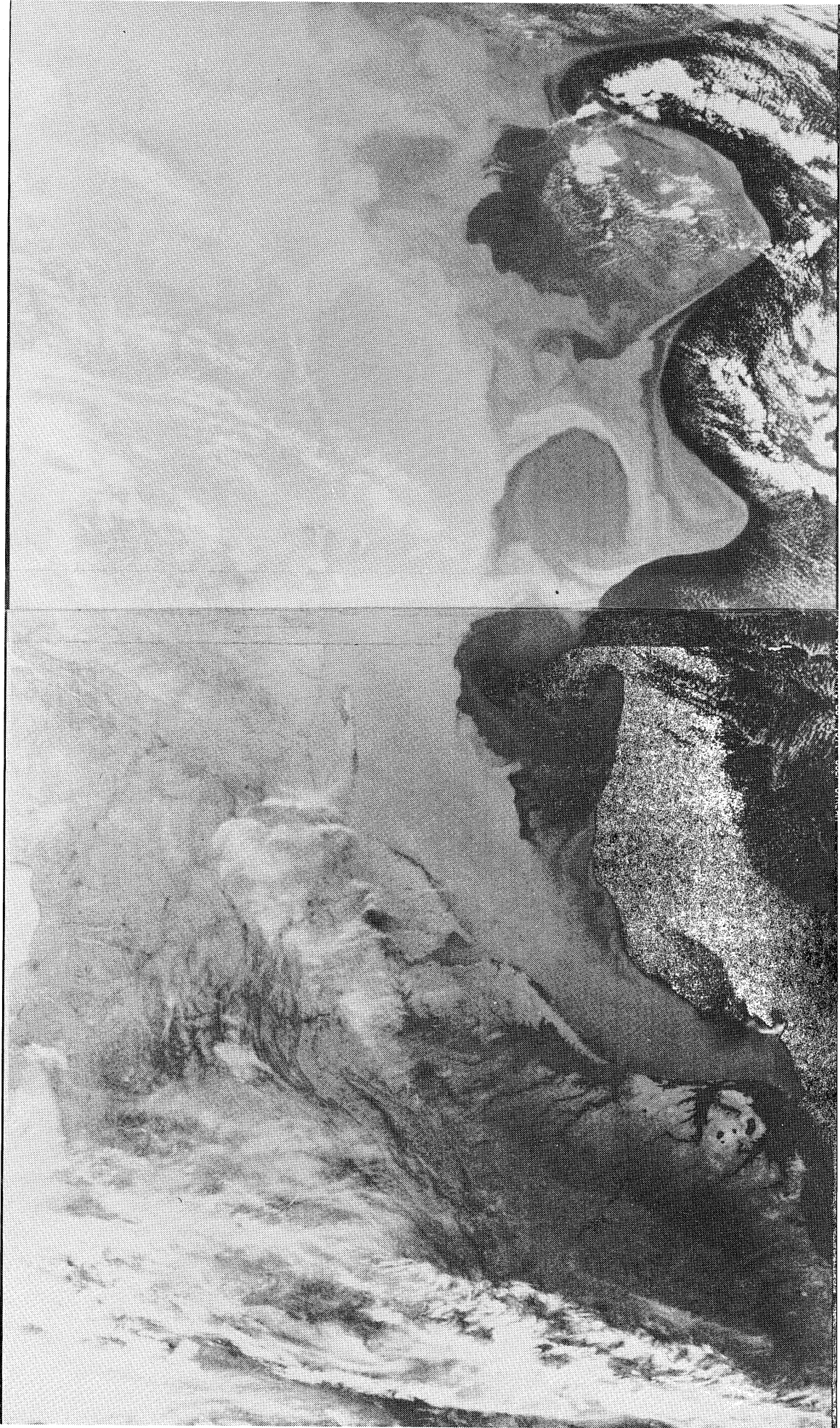


Fig. 8. Structure associated with the north wall of the Gulf Stream south of Cape Cod and Nova Scotia on 28 April 1974. Warm core eddies form and move west in the edge of the colder shelf water.

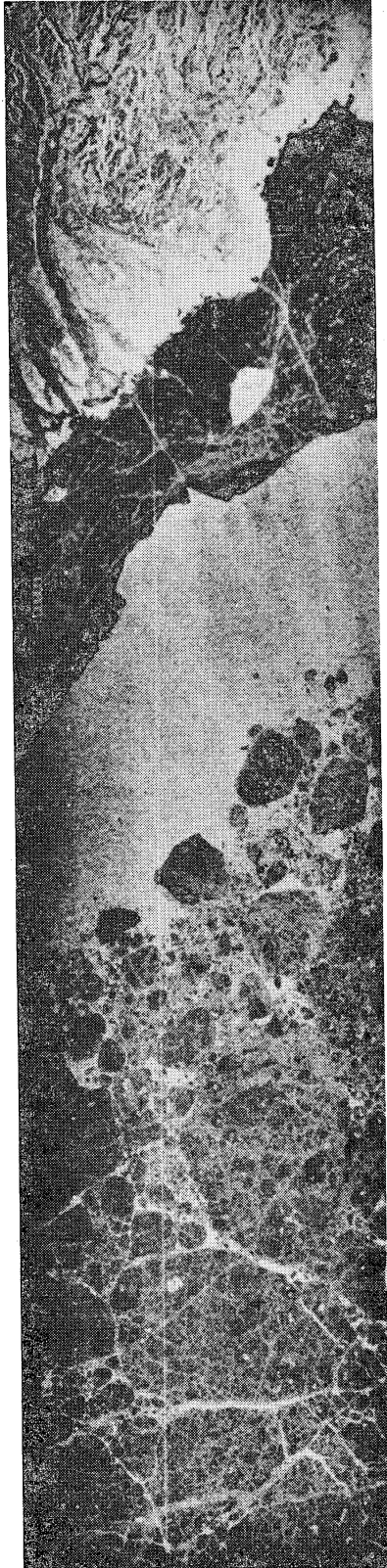


Fig. 9. Optically processed Seasat SAR image of an area 18 by 75 miles showing from left to right (west to east) sea ice floes, open water, shorefast ice and the coast of Banks Island, Canada.

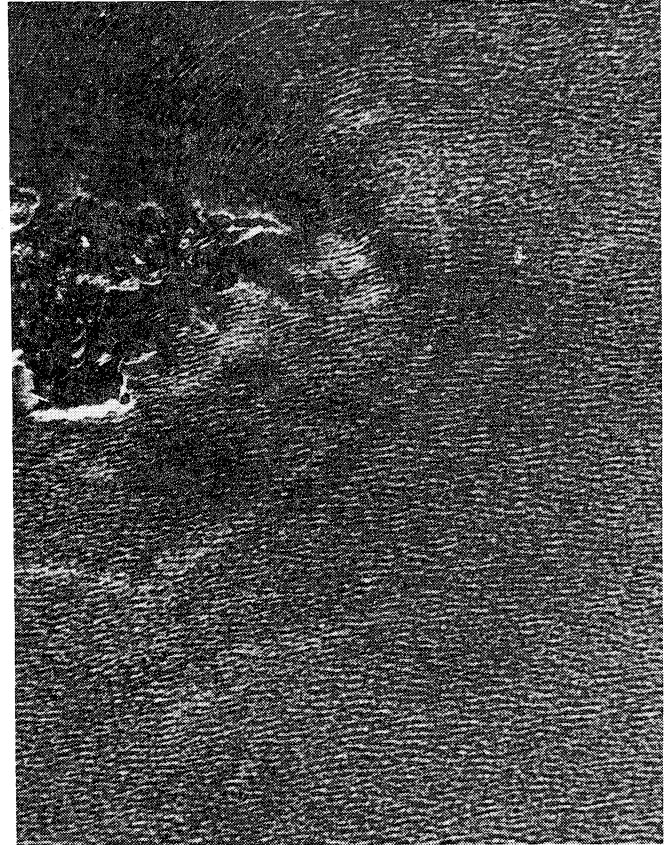


Fig.10. Digitally processed Seasat SAR image of Sumburgh Head at the southern tip of the Shetland Islands, northeast of Scotland on 15 September 1978. (North is up.) Ocean waves of 205 m wavelength are seen arriving from the west and diffracting round the head.



Fig. 11. Scatterometer wind vectors (with two- and four-fold ambiguities) as observed over the north Atlantic on 22 August 1978. These are interpreted as a cyclone-col-cyclone pattern as shown.

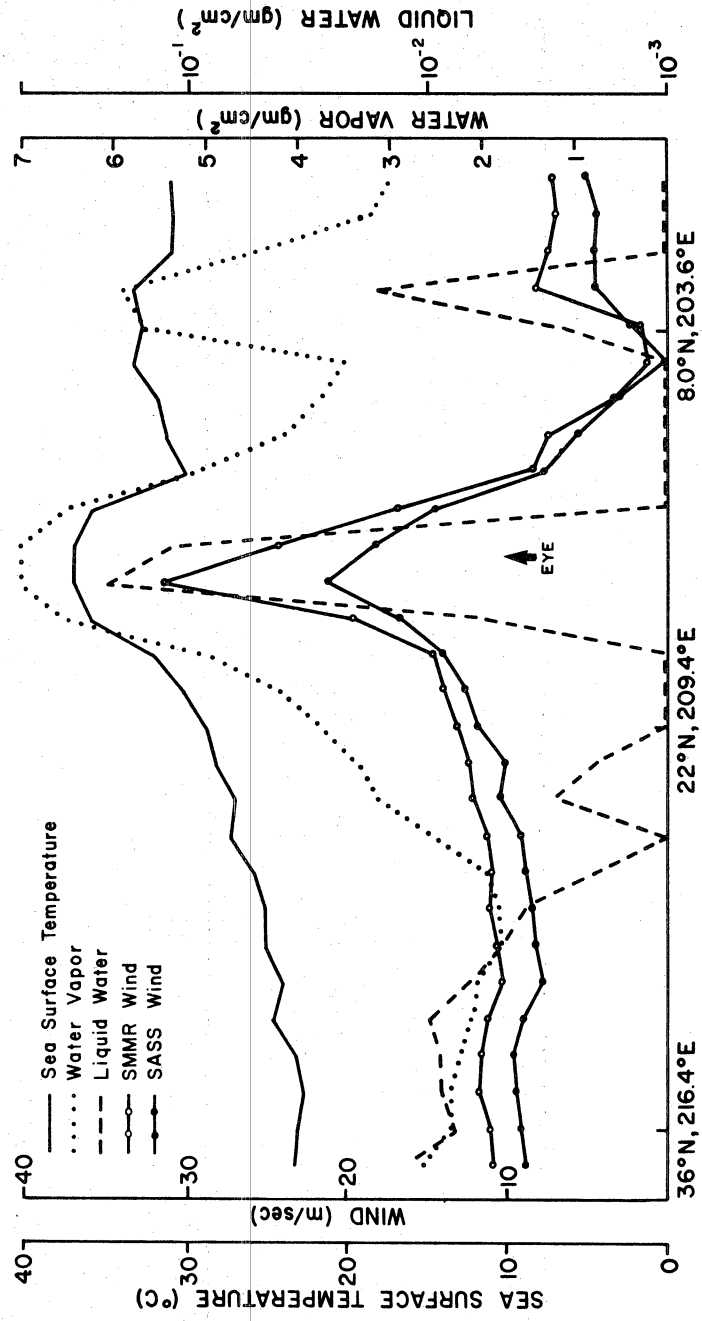


Fig. 12. Profiles of sea surface temperature, surface wind speed and total atmospheric water vapour and liquid water content calculated from SEASAT radiometer (SMMR) data. The comparison with scatterometer wind measurements shows the advantage of radiometer data in allowing correction for atmospheric effects.

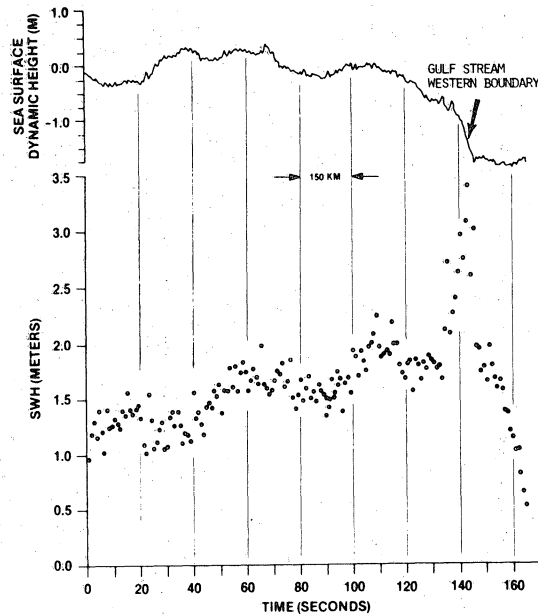


Fig. 13. Sea surface dynamic heights and significant wave heights calculated from Seasat altimeter data collected on 28 September 1978.

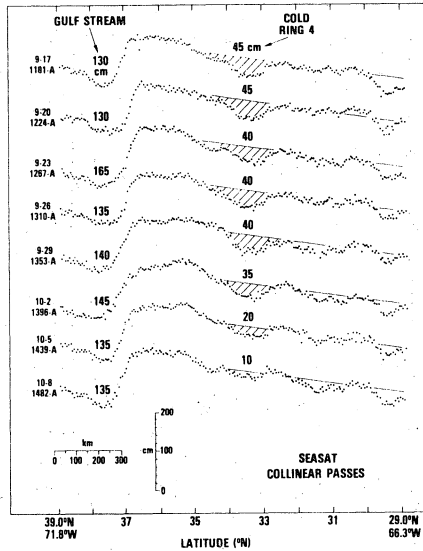


Fig. 14. Sea surface dynamic heights from eight passes of Seasat altimeter data over the same track crossing the Sargasso Sea and then the Gulf Stream from southeast to northwest. Passes are at three-day intervals and initially (top) show a cold ring causing a 40 cm depression of the sea surface. This depression becomes less as the ring moves out from beneath the satellite.